Physica Scripta

RECEIVED
16 July 2021

REVISED
10 October 2021

ACCEPTED FOR PUBLICATION
27 October 2021

PUBLISHED
8 November 2021

PAPER

# Time-resolved evolution of collisional transient sheath in plasma source ion implantation

J Taghinejad, A R Niknam, A R Rastkar and H Ghomi

Laser and Plasma Research Institute, Shahid Beheshti University, 1983969411, Tehran, Iran

E-mail: a-niknam@sbu.ac.ir

Keywords: transient sheath, sheath expansion, plasma source ion implantation, current density, time-resolved dynamics

## Abstract

In this work, an analytical model for the time-resolved dynamics of the collisional transient sheath in the plasma source ion implantation (PSII) process is developed. The presented model can forecast the temporal dependence of the implanted ion flux and sheath width in the collisional transient sheath. During the PSII process, the effects of some physical parameters such as applied voltage and gas pressure on the pattern of sheath growth are discussed. It is found that the ion flux can get higher values by increasing the gas pressure during the matrix sheath while the dynamics of ions in the expanding sheath are restricted to the collisionality condition, and ion flux is reduced impressively. Moreover, these results are demonstrated that the increase of the applied voltage causes the high rate of sheath expansion and electric field and then ion flux. The final value of the ion velocity in the expanded sheath tends to the ion Bohm velocity.

## 1. Introduction

The coating materials and surface treatments are becoming important for tribological applications, repairing the surfaces, protecting the surfaces from conditions of stress and corrosive media, etc. One of the most promising techniques of surface treatment of materials is plasma source ion implantation (PSII), or plasma immersion ion implantation (PIII) [1–6]. The PSII method is employed in the material surface processing, manufacturing of large-scale integrated circuits (ICs), and fabrication of semiconductor devices [2, 7]. In the conventional ion beam implanter, to achieve uniform implantation, the beam is electrically scanned and the target object is mechanically rotated while in PSII method, a series of negative high-voltage pulses are applied to a sample (target) immersed in plasma and then a transient sheath layer is developed around the target [8]. Hence, the understanding of the time-resolved dynamics of the transient sheath in the PSII process is important [9]. In the PSII process, the ions are extracted from the plasma and accelerated into the target through a transient sheath directly [10]. In this way, the ions from the plasma are implanted in the target with a relatively uniform spatial distribution [11]. Furthermore, in the PSII technique, the achievable dose rate is tens of times greater than other conventional ion implantation systems and this technique even could be done in low energies [12]. The energetic ions injected into the surface of a solid target cause the atomic composition and structure of the topmost surface to change. Therefore, new surface layers are created with improved resistance to wear, corrosion, and fatigue [13].

As stated in the above paragraph, in the PSII technique, the target is placed in a high-density plasma subjected to negative high voltage pulses [14]. When a negative voltage is applied to the target, the electrons are expelled away from the target region [15]. This process occurs in the time scale of the inverse electron plasma frequency, and as a result, an ion matrix sheath is formed between the target and the plasma [16]. Then, due to the non-neutral distribution of the charges, the electric field in the sheath region can be raised [17, 18]. The created electric field can accelerate the ions to high energy toward the target on the time scale of the inverse ion plasma frequency [19]. As time passes, the charge imbalance forces the sheath-plasma edge farther away, and on a still longer time scale, the system evolves toward a steady-state Child law sheath [20]. The initial width of the sheath is determined by the amplitude of the applied potential. Consequently, the applied voltage influences the

© 2021 IOP Publishing Ltd

ion dynamics at this regime [21]. Ion's dynamics are described by laws of ion space-charge sheath. The sheath expands while the target bias voltage varies from zero to a constant negative value [22]. At this time, ion dynamics could be determined by continuity and momentum transfer equations in the fluid model. On a longer time scale, the system transit to the steady-state Child law sheath. So, ion's dynamic is followed by Child-Langmuir laws [2, 23]. The whole process, which occurs in the sheath behavior of the PSII process, is investigated to forecast the ion dynamics [24]. The different ranges of applied voltages that lead to the various ion dynamics are described by different laws of ion space-charge sheath [25]. In all ranges of pressure (collisionless and collisional regimes), plasma bulk, and sheath layer dynamics must be joined at their interface [26]. The sheath and plasma bulk join smoothly at a sufficiently high-pressure collisional regime, while a transition layer is required for joining at low pressures [27, 28]. So, for different ranges of collisionality, the sheath expansion is varied [29]. Moreover, the ion flux and the rate of implanted ion dose have a variant range [30]. The ion flux uniformity can be improved by adjusting the pulse width and applied potential [31]. However, the sheath region is the most important to PSII and its behavior should be discussed in applied potentials and pressures [32]. Sheridan *et al*, [17] have presented an approximate theory of the collisional transient sheath spanning. They have used the steady-state Child's law-like expression presented by Reimann *et al* [18] in which the initial matrix sheath was neglected. Benilov has tried to trace the footprint of the Child-Langmuir model of a collisionless electron-free ion sheath with the ion velocity, electric field, and potential vanishing at the sheath edge [16]. A collisionless model for PIII has been demonstrated by Lieberman [2]. The author tried to obtain analytically ion flux for the collisionless sheath.

During the past decades, many researchers have studied the spatial evolution of sheath in the plasma and little attention has been paid to the temporal evolution of sheath. In this study, we present an analytical model to describe the dynamics of the collisional transient sheath in the PSII process for an applied rectangular voltage pulse at planar geometry. There are two methods for describing the collision: (1) the regime of the constant mean free path and (2) the regime of constant collision frequency [33–35]. Here we consider the regime of the constant mean free path. Moreover, for a collisional plasma, the ion-neutral mean free path is less than the Debye length, $\lambda_i \leqslant \lambda_D$. Hence, the sheath-presheath boundary is not very definite and can extend into the bulk plasma because of collision. Therefore, we ignore the presheath region [3, 37]. The presented analytical model evaluates the physics of sheath width evolution (initial matrix sheath, expanding sheath, and expanded sheath) and formulates implantation ion current density during applied pulse width. Moreover, we investigate the effect of physical parameters such as gas pressure and applied voltage on mechanisms of implanted current density and dynamics of sheath edge position that are useful in describing the PSII process. We show that the gas pressure parameter can increase the implanted current density in the initial matrix sheath. Then, with the passage of time, the ion-neutral collision in the expanding sheath becomes important (ion mean free path less than sheath width), so the ion implantation current is reduced. We also indicate that the amplitude of applied voltage as another determinative parameter of ion motions affects the implantation current density and the sheath width.

## 2. Theoretical model and sheath motion equations

We consider a planar target immersed in a uniform plasma of density $n_0$. A pulsed voltage with amplitude of $-V_0$ and time width $t_p$ is applied to the target at time $t = 0$. The electrons near the surface are driven away and a uniform matrix sheath is formed on the time scale of the inverse electron plasma frequency. The applied voltage is much greater than the electron temperature $T_e$ where $T_e$ is now expressed in volts [3]; hence the Debye length is much less than the initial matrix sheath width i.e., $\lambda_D \ll s_0$. Then, ions within the sheath are accelerated into the target on the time scale of the inverse ion plasma frequency. Consequently, the sheath edge moves away from the cathode while exposing new ions that are extracted. In this case, the entry velocity of the ions to the sheath region is $u_b + ds/dt$ which is the sum of velocities of Bohm and sheath edge motion. Finally, with the passage of long time, the system evolution tends toward a steady-state Child law sheath [2]. A schematic diagram showing these processes is presented in figure 1. As depicted in figure 1, the initial sheath width is $s_0$, and as time goes on, the sheath boundary increase by the slope of $ds/dt$. Hence, the time dependence of the sheath width can be found by assuming quasi-static sheath expansion [1] which can be written as

$$s(t) = s_0 + \frac{ds}{dt}t. \tag{1}$$

The ion current demanded by steady-state Child law sheath is supplied by the number of uncovered ions at the expanding sheath edge and by the drift of ions toward the target at the Bohm speed (ion-sound velocity). In other words, the charge per unit time crossing the sheath-plasma boundary is as follows:

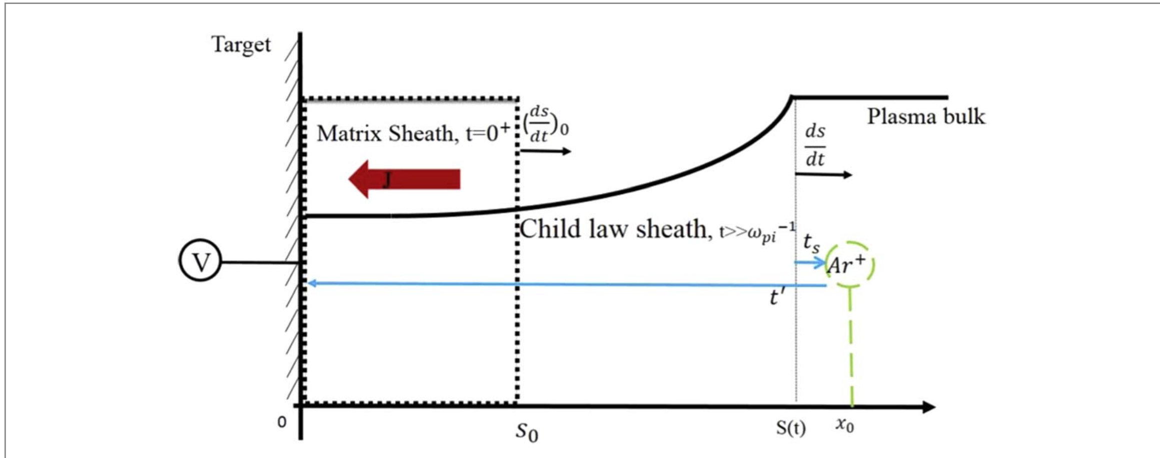


**Figure 1.** The formation of the matrix sheath (dashed line) and the evolution of the quasi-static Child law sheath (stretch line) in the planar PSII.

$$J_c = en_0\left(u_b + \frac{ds}{dt}\right), \tag{2}$$

where $u_b$ is the Bohm speed and $n_0$ is the initial plasma density. Therefore, to calculate the temporal dependence of the implanted ion current density at the surface of the target, we use collisional sheath evolution law as [3]. In the routine PSII process where ion-neutral collisions are dominant the Child law current density $J_c$ is obtained as

$$J_c = \left(\frac{500}{243\pi}\right)^{\frac{1}{2}} \varepsilon_0 \left(\frac{2e\lambda_i}{M}\right)^{\frac{1}{2}} \frac{V_0^{\frac{3}{2}}}{s^{\frac{5}{2}}}, \tag{3}$$

where $\lambda_i$ is the ion mean free path, $M$ is the ion mass, $e$ is the electron charge, and $\varepsilon_0$ is the free space permittivity. In the collisional regime, the mean free path is smaller than the sheath width. By equating equations (2) and (3) one can find the sheath expanding velocity for a planar geometry as below:

$$\frac{ds}{dt} = \left(\frac{125}{243\pi}\right)^{\frac{1}{2}} \frac{\lambda_i^{\frac{1}{2}} s_0^2 u_0}{s^{\frac{5}{2}}} - u_b \tag{4}$$

where $u_0 (= \sqrt{2eV_0/M})$ is the characteristic ion velocity and by inserting equation (4) into equation (1), one can obtain the time-varying sheath width $s(t)$ and consequently can determine the implanted current density $J(t)$. As above mentioned, during and after matrix sheath ion implantation, quasi-static Child law sheath forms to expanding sheath ion implantation. Therefore, in the following subsections, we will investigate the matrix sheath implantation and the Child law sheath implantation.

## 3. A. Matrix sheath implantation

Due to the initial uniform charge distribution in the matrix sheath, the electric field varies linearly with $x$ (ion's position). Therefore, using Newton's second law and the Krook's collisional term, we have

$$\frac{d^2x}{dt^2} = \omega_{pi}^2(x - s) - \nu_m \frac{dx}{dt}, \tag{5}$$

where $\omega_{pi}$ is the ion plasma frequency, and $\nu_m$ is the ion collision frequency. By combining equations (1), (4) and (5) we obtain a differential equation for the ions position as follows:

$$\frac{d^2x}{dt^2} = \omega_{pi}^2 x - \nu_m \frac{dx}{dt} + \left[u_b \omega_{pi}^2 t - \omega_{pi}^2 s_0 - \omega_{pi}^2 t \left(\frac{125}{243\pi}\right)^{\frac{1}{2}} \frac{\lambda_i^{\frac{1}{2}} s_0^2 u_0}{s_0^{\frac{5}{2}}}\right]. \tag{6}$$

equation (6) is completely universal for the high pressure (collision-dominated) sheaths. By neglecting the Bohm velocity and $\nu_m \longrightarrow 0$, this equation reduces to the equation presented in reference [2] for the collisionless plasma. Now integrating equation (6), we find

$$x = e^{-t\zeta^+} - \frac{t\beta u_b - \alpha u_0}{\beta} + \frac{2\beta\omega^2 s_0 - \beta\nu_m u_b + \alpha u_0 \nu_m}{\beta\omega^2} - e^{-t\zeta^-}$$

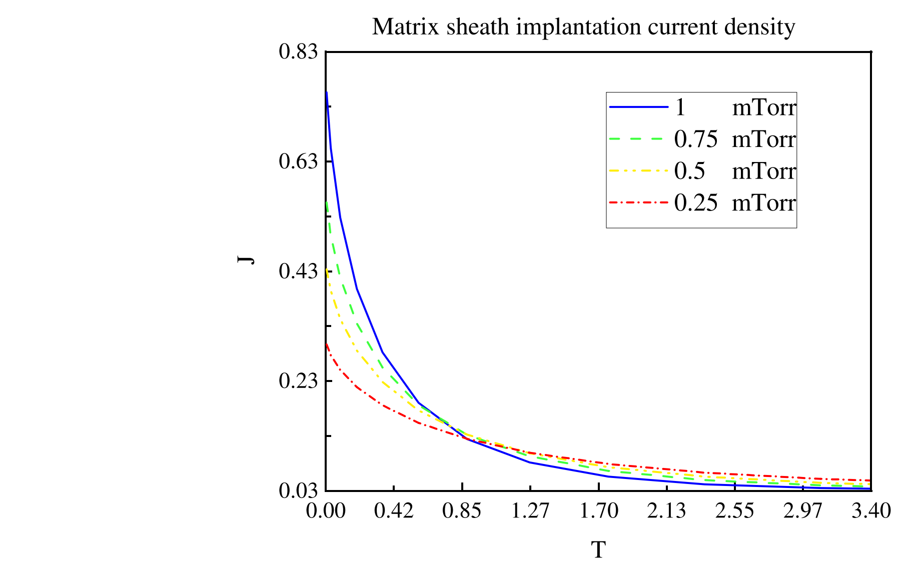


**Figure 2.** The normalized implanted current density of the matrix sheath as a function of the normalized time for gas pressures of 0.25, 0.5, 0.75, and 1mTorr at the voltage of 6 kV.

$$\times\left(\frac{2\beta u_b + 2\beta x_0 + \beta(\nu_m^2 + 4\omega^2)^{\frac{1}{2}} + \beta\nu_m - 2\alpha\lambda^{\frac{1}{2}}u_0}{\beta}\right)(\nu_m - (\nu_m^2 + 4\omega^2)^{\frac{1}{2}}), \tag{7}$$

where $\alpha = 5(15\lambda_i)^{1/2}/s_0^{1/2}$, $\beta = 27\pi^{1/2}$, $\zeta^+ = \frac{1}{2}\left(\frac{\nu_m}{2} + \nu_m^2 + 4\omega^2\right)^{1/2}$, and $\zeta^- = \frac{1}{2}\left(\frac{\nu_m}{2} - \nu_m^2 - 4\omega^2\right)^{1/2}$. $x_0$ is the initial particle position and $dx/dt = 0$ at $t = 0$. Inserting $x = 0$ in equation (7), we can calculate the ion flight time, $t$, across the matrix sheath from the below equation

$$e^{-t\zeta^+} - e^{-t\zeta^-}\frac{2\beta u_b + 2\beta x_0 + \beta(\nu_m^2 + 4\omega^2)^{\frac{1}{2}} + \beta\nu_m - 2\alpha\lambda^{\frac{1}{2}}u_0}{\beta}(\nu_m - (\nu_m^2 + 4\omega^2)^{\frac{1}{2}})$$
$$-\frac{t\beta u_b - \alpha u_0}{\beta} + \frac{2\beta\omega^2 s_0 - \beta\nu_m u_b + \alpha u_0\nu_m}{\beta\omega^2} = 0. \tag{8}$$

By differentiating equation (8) with respect to $t$ we obtain

$$\frac{dx_0}{dt} = \frac{1}{2}(-\zeta^+ e^{-t\zeta^+}e^{t\zeta^-})$$
$$+\left(\zeta^- e^{-t\zeta^+}e^{t\zeta^-} - u_b e^{t\zeta^-} - \zeta^- e^{t\zeta^-}\left(\frac{\beta u_b - \alpha u_0}{\beta}\right)\right)(\nu_m - (\nu_m^2 + 4\omega^2)^{\frac{1}{2}})^{-1}. \tag{9}$$

In this work, we considered a high-voltage sheath with $V_0$ much greater than the electron temperature $T_e$, and we also assumed that during the ion motion in the sheath the electric field is frozen at its initial values, except the changes related to the moving sheath velocity [2]. Therefore, using equation (9), one can calculate the implanted current density, $j = en_0(dx_0/dt)$, as a function of $t$ and consequently, the normalized implanted current density $J = j/(en_0u_0)$, versus the normalized time $T = t\omega_{pi}$. By inserting $x_0 = s_0$ in equation (8), we obtain $T \simeq 3.4$. Hence, all matrix sheath ions at $0 \leqslant T \leqslant 3.4$ are implanted. Figures 2 and 3 show the plot of $J$ as a function of $T$ at this period of time.

On the other hand, the temporal evolution of the current density in the sheath region causes a change in the sheath potential. In the high-voltage sheath, the ionization within the sheath region is negligible and the current continuity can be written as $n_i u_i = n_s u_s$ where $n_s$ and $u_s$ are the values due to the sheath edge. Moreover, in a collisional plasma sheath, the ion motion can be expressed as $u_i \cong \mu_i E$ where $\mu_i (= 2e\lambda_i/\pi M|u_i|)$ is the ion mobility. Hence, $u_i$ is calculated as follows:

$$u_i = \frac{2e\lambda_i}{\pi M|u_i|}E. \tag{10}$$

By considering constant $\lambda_i$ at intermediate pressures and solving for $u_i > 0$, we have

$$n_i = n_s u_s\left(\frac{\pi M}{2e\lambda_i E}\right)^{1/2}, \tag{11}$$

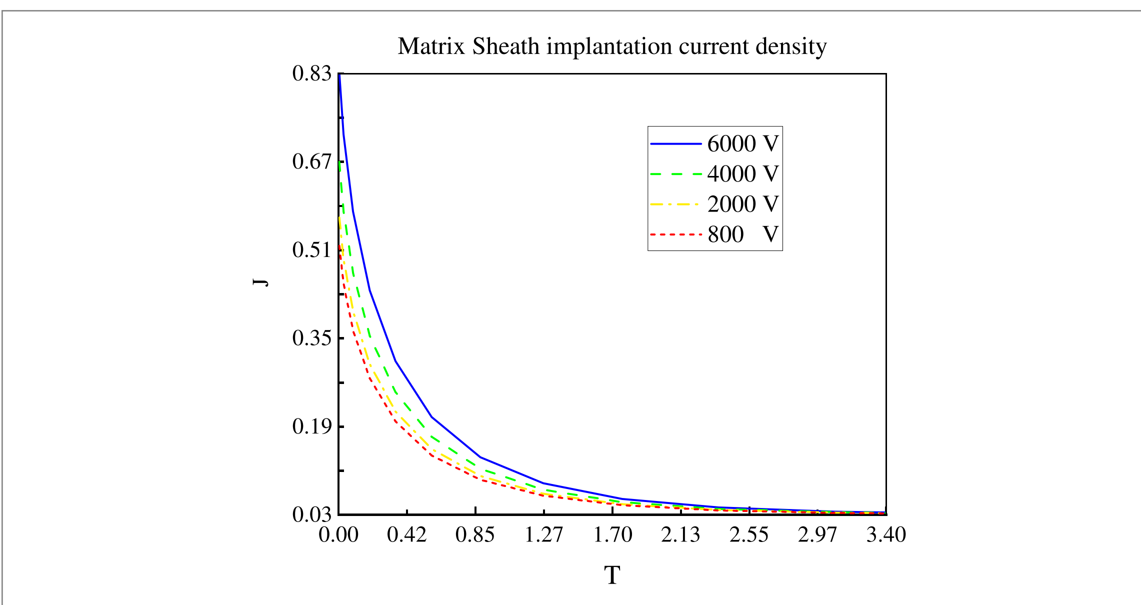


**Figure 3.** The normalized implanted current density of the matrix sheath as a function of the normalized time for voltages of 800, 2000, 4000, and 6000 $V$ at the gas pressure of 1mTorr.

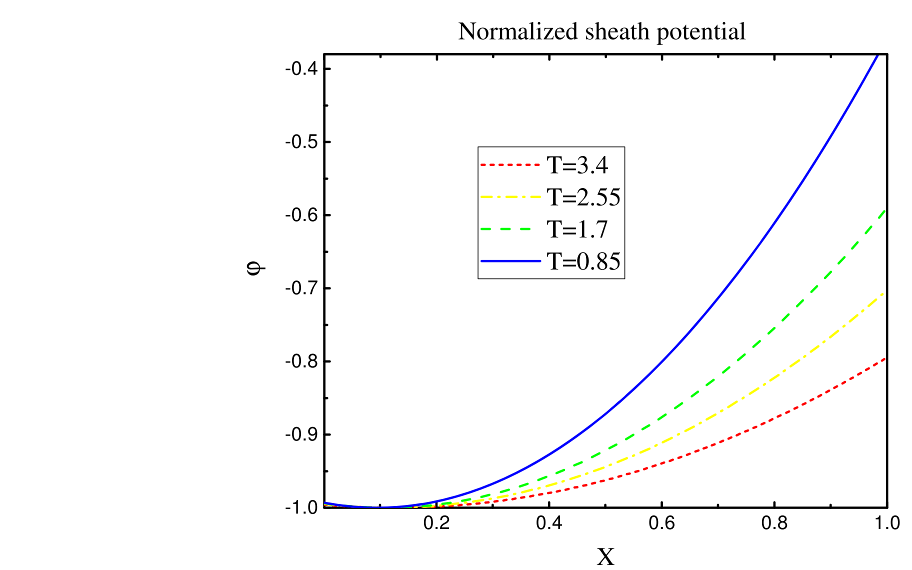


**Figure 4.** The normalized sheath potential of the matrix sheath as a function of X for the normalized times of 0.85, 1.7, 2.55, and 3.4 at gas pressures of 0.75mTorr and voltage of 6 kV.

and inserting $n_i$ in Gauss' law, we obtain

$$E^{1/2}\frac{dE}{dx} = \frac{en_s u_s}{\varepsilon_0}\left(\frac{\pi M}{2e\lambda_i}\right)^{1/2}. \tag{12}$$

Then, by integrating the equation $E = -d\phi/dx$ and the condition $\phi = -V_0$ at $x = 0$, the sheath potential is obtained as follows:

$$\phi(x) = -\frac{3}{5}\left(\frac{3en_s u_s}{2\varepsilon_0}\left(\frac{\pi M}{2e\lambda_i}\right)^{1/2}\right)^{2/3}(s_0 - x)^{5/3}. \tag{13}$$

Using this equation, the spatial evolution of the electric potential in the matrix sheath is plotted in figure 4.

## 4. B. Child Law Sheath Implantation

In the Child law sheath, the implanted ions have initial positions greater than initial sheath width ($x_0 > s_0$). So, additional time $t_s$ needed for the initial sheath edge at $s_0$ reach to $x_0$. In other words, during $t_s$, the sheath width expands and reaches the ion initial position as depicted in figure 1. The time $t_s$ can find from equation (4) accurately. For calculation, equation (4) can be rewritten as follows:

$$\frac{ds}{\left(\frac{125}{243\pi}\right)^{\frac{1}{2}}\frac{\lambda_i^{\frac{1}{2}} s_0^2 u_0}{s^{\frac{5}{2}}} - u_b} = dt. \tag{14}$$

Since $((125/243\pi)^{1/2}\lambda_i^{1/2} s_0^2 u_0/s^{5/2}) \gg u_b$, one can obtain

$$t_s = \frac{x_0^{\frac{7}{2}}}{\frac{7}{2}\left(\frac{125}{243\pi}\right)^{\frac{1}{3}}\lambda_i^{\frac{1}{2}} s_0^2 u_0}. \tag{15}$$

Equation (15) presents an apparent dependence on ions position, $x_0$. At time $t_s$ an ion at the sheath edge starts its flight through the sheath. Thus, using the conduction current density, $j = en_0 u(x)$, applied to the Gauss' law ($E = enx/\varepsilon_0$) and integrating, these lead to

$$\frac{dE}{dt} = \left(\frac{500}{243\pi}\right)^{\frac{1}{2}} en_0 \left(\frac{2e\lambda_i}{M}\right)^{\frac{1}{2}} \frac{V^{\frac{3}{2}}}{s^{\frac{5}{2}}}. \tag{16}$$

Using $E = -\nabla V$ and $s$ variation from 0 to $x_0$, we obtain the time $t'$ as follows:

$$t' = \frac{3}{u_0\left(i\frac{12\pi}{125\lambda_i}\arctan(i\eta) + \frac{\eta}{x_0}\right)}, \tag{17}$$

where $t'$ is so-called ion flight time across the sheath and $\eta = \sqrt{\frac{12\pi}{125\lambda_i}x_0 + 1}$ is a dimensionless parameter. In the collisionless limit, the equation (17) reduces to the equation presented in reference [2]. Figure 1 shows schematically $t'$, $t_s$, and theirs intervals. Also, the total time for an ion to reach the target surface from initial position ($x_0$) is given by

$$t = t' + t_s. \tag{18}$$

Instituting equations (15) and (17)into equation (18), we have

$$t = \frac{3}{u_0\left(i\frac{12\pi}{125\lambda_i}\arctan(i\eta) + \frac{\eta}{x_0}\right)} + \frac{x_0^{\frac{7}{2}}}{\frac{7}{2}\left(\frac{125}{243\pi}\right)^{\frac{1}{3}}\lambda_i^{\frac{1}{2}} s_0^2 u_0}. \tag{19}$$

Differentiating equation (19) leads to implanted ion velocity in the expansion sheath as follows:

$$\frac{dx_0}{dt} = \left(\frac{7}{2}\right)^{-5/7}\left(\left(\frac{125}{243\pi}\right)^{\frac{1}{2}}\lambda_i^{\frac{1}{2}} s_0^2 u_0\right)^{\frac{2}{7}}$$

$$+\frac{\left(\frac{3\eta}{125\lambda_i}\right)^{\frac{1}{2}}}{s_0 x_0^2} - \frac{\frac{12\pi}{125\lambda_i}}{\eta} u_0\left(i\frac{12\pi}{125\lambda_i}\arctan(i\eta) + \frac{\eta}{x_0}\right). \tag{20}$$

This equation shows the explicit dependence of the implanted ion velocity and consequently, the normalized implantation current density, $J = (dx_0/dt)/u_0$, on $\lambda_i$. This current density as a function of time is plotted in figures 5 and 6.

The sheath potential in the Child law sheath can be calculated by the current density of the Child law sheath (equation (20)), time-dependent sheath width, and Gauss' law. As in the matrix sheath subsection, by integration of Gauss' law, the sheath potential is obtained as follows:

$$\phi(x) = -\frac{3}{5}\left(\frac{3en_s u_s}{2\varepsilon_0}\left(\frac{\pi M}{2e\lambda_i}\right)^{1/2}\right)^{2/3}(s - x)^{5/3}. \tag{21}$$

The spatial evolution of the electric potential in the Child law sheath is plotted in figure 7.

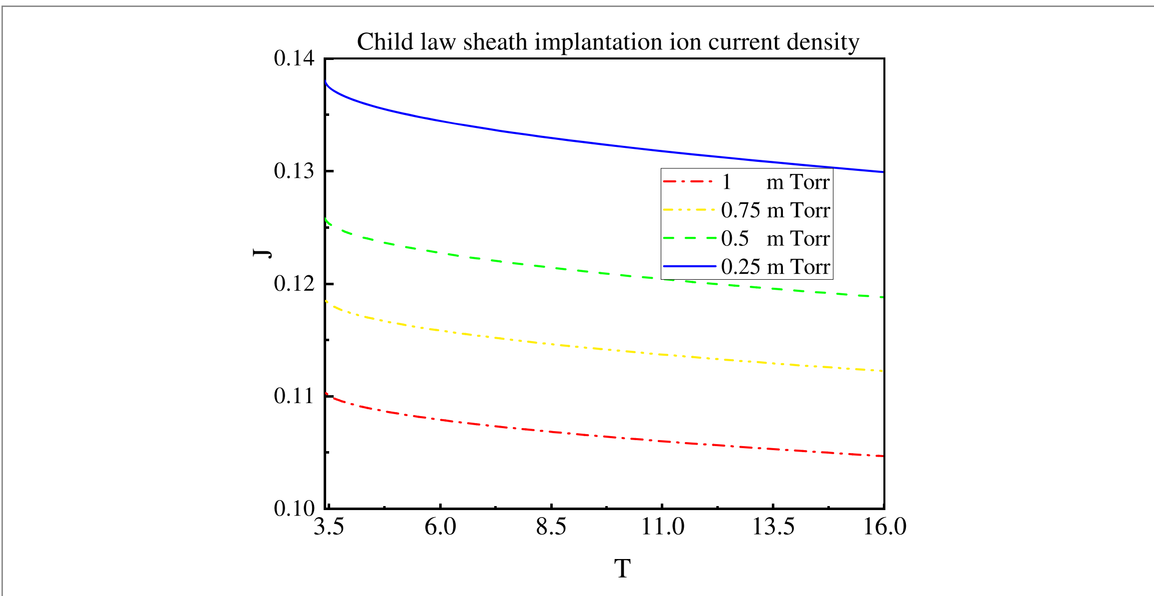


**Figure 5.** The normalized implanted current density of the Child law sheath as a function of the normalized time for gas pressures of 0.25, 0.5, 0.75, and 1mTorr at the voltage of 6 kV.

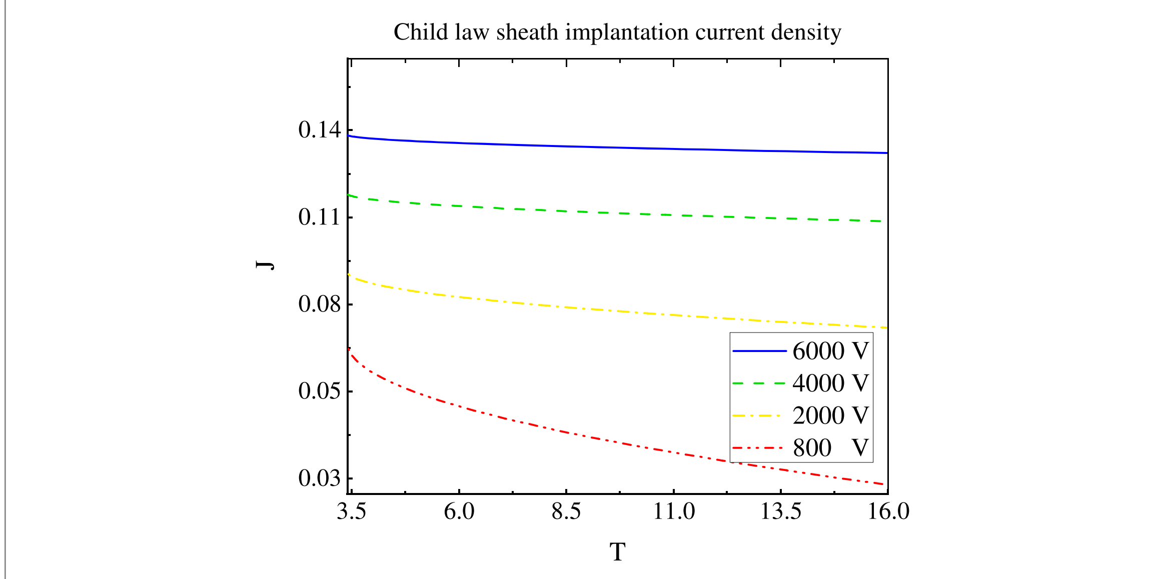


**Figure 6.** The normalized implanted current density of the Child law sheath as a function of the normalized time for voltages 800, 2000, 4000, and 6000 $V$ at the gas pressure of 0.25mTorr.

## 5. Results and discussion

In this section, we analyze the results for the development of collisional sheath propagation during a pulse width for PSII process near a planar target. Our simulations begin with initial conditions of $t = 0$ and $s = s_0$ (ion matrix sheath), and solve equations (9) and (20)numerically until the time at which the pulse is turned off. The neutral gas used for this process is argon. The plasma density and the electron temperature are $n_0 = 1 \times 10^9\ \mathrm{cm}^{-3}$ and $T_e = 1.4eV$, respectively, and the amplitude of the applied potential is $V_0 = 6kV$ which is greater than the electron temperature. Therefore, the initial sheath thickness for these parameters becomes $s_0 = \sqrt{2\varepsilon_0 V_0/en_0} = 0.028$ m. The charge exchange cross-section $Q \cong 4.0 \times 10^{15}\ \mathrm{cm}^2$ for Ar is used. For the neutral gas pressures of 0.25, 0.5, 0.75, and 1mTorr, the ion-neutral mean free path, $\lambda_i = (\sqrt{2}\, n_0 Q)^{-1}$, are 0.04, 0.03, 0.025, and 0.02 cm, respectively (see [36–38]). All the parameters selected are based on the experimental literature in the collisional region ($s \geqslant \lambda_i$). Using equation (9) and setting $x = 0, x_0 = s_0$ and $\lambda_i = 0.03$ cm, we get the time interval due to the matrix sheath. This means is that after a bias voltage is supplied to a conducting target, ions in the matrix sheath can be implanted in the target during $0 < T < 3.4$. These processes are shown in figures 2 and 3. Figure 2 presents the normalized implantation current density $J = j/en_0u_0$ versus the normalized time $T = t\omega_{pi}$ for different gas

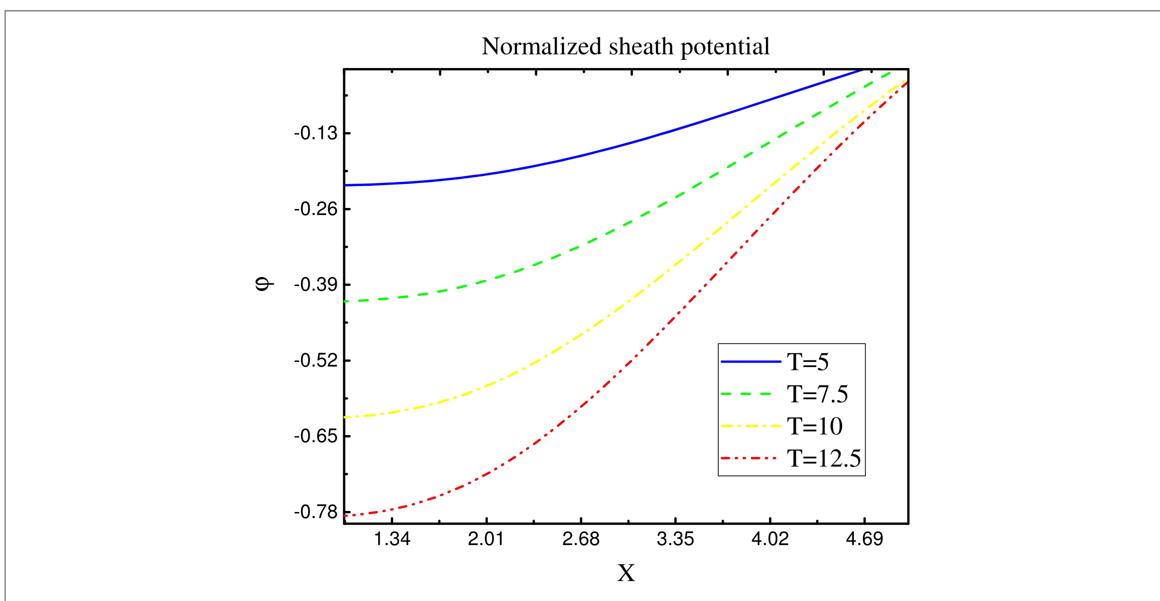


**Figure 7.** The normalized sheath potential of the Child law sheath as a function of X for the normalized times of 5, 7.5, 10, and 12.5 at gas pressures of 0.75mTorr and voltage of 6 kV.

pressures (different mean free paths) in the matrix sheath. The results show that in the uniform matrix sheath as the gas pressure increases, the initial onset of ion flow to the target surface elevates. During and after matrix sheath implantation, a quasi-static Child law sheath forms As time evolves, the sheath width in the expanding sheath becomes greater than the mean free path. Therefore, the ion-neutral collision has an important role in ion transition, and so the ion current density suddenly falls down. On the other hand, by increasing the amplitude of applied pulse, ions in the expanded sheath get the appropriate energy to reach the target surface (see figure 3). Figure 4 shows the normalized sheath potential of the matrix sheath, $\varphi = \phi/V_0$, as a function of the normalized spatial length, $X = x/s_0$ for the normalized times of 0.85, 1.7, 2.55, and 3.4 at gas pressures of 0.75 m Torr and voltage of 6 kV. For the matrix sheath region, we have $0 \leqslant x \leqslant s_0$. This figure indicates that the slope of the curves of matrix sheath potential decreases over time.

In the initial stage of ion implantation, the energy distribution of the ions depends on their initial position in the sheath. The matrix sheath thickness is considered as the initial sheath width. Then, for $T > 3.4$, the ions response to the electric field variation and the sheath expands adiabatically. Plasma ions arriving at the sheath edge are accelerated by the sheath's electric field and extracted from the plasma. The sheath edge proceeds into the plasma and its thickness increases. Figure 5 indicates the dimensionless current density profiles as a function of the normalized time in the Child law sheath for different gas pressures. As this figure displays, while the gas pressure increases and consequently the ion mean free path and the ion energy decrease, the current density reduces. Figure 6 shows the temporal evolution of implanted current density in the Child law sheath for different applied voltages. From this figure, one can see that the implanted current density raises by increasing the applied voltage. Moreover, the increase of applied voltage results in an increase in ion energy. Then the energetic ion reaches the target surface and implants into the target. Figure 7 shows the potential profiles for four different times in the Child law sheath. This figure indicates that the slope of the curves of Child law sheath potential increases by time due to the sheath edge motion.

The temporal evolution of the sheath width for gas pressures of 0.25, 0.5, 0.75, and 1mTorr is presented in figure 8. This figure shows that the sheath width increases with time and decreases with the increase of gas pressure. Therefore, by increasing the gas pressure, the collisions become important and the rate of sheath expansion slows, and the sheath width tends to a constant value, especially at higher pressures. This constant value can be obtained using equation (4) when $ds/dt \to 0$. In this case, we have $s(=((125/243\pi)^{1/2}(\lambda_i^{1/2} s_0^2 u_0)/u_b)^{2/5}) \gg s_0$. Finally, in figure 9, we plot the total implantation current density as a function of normalized time at gas pressure of 0.4 mTorr and $V_0 = 6kV$ which is in good agreement with presented results in other literatures (see references [5] and [17]). According to physical timescales, three different phases (initial matrix sheath, expanding sheath, and expanded sheath) can be distinguished from figure 9. When a negative high-voltage pulse is applied to the target, a matrix sheath is initially formed for $T < 3.4$ (blue line). Then during and after the matrix sheath i.e, for $T > 3.4$, the expanding sheath is formed (red line). And on a longer time scale ($T \to \infty$), one can see the expanded sheath and in this case, the implantation current density evolves toward a steady-state value i.e., $J(\infty) \neq 0$.

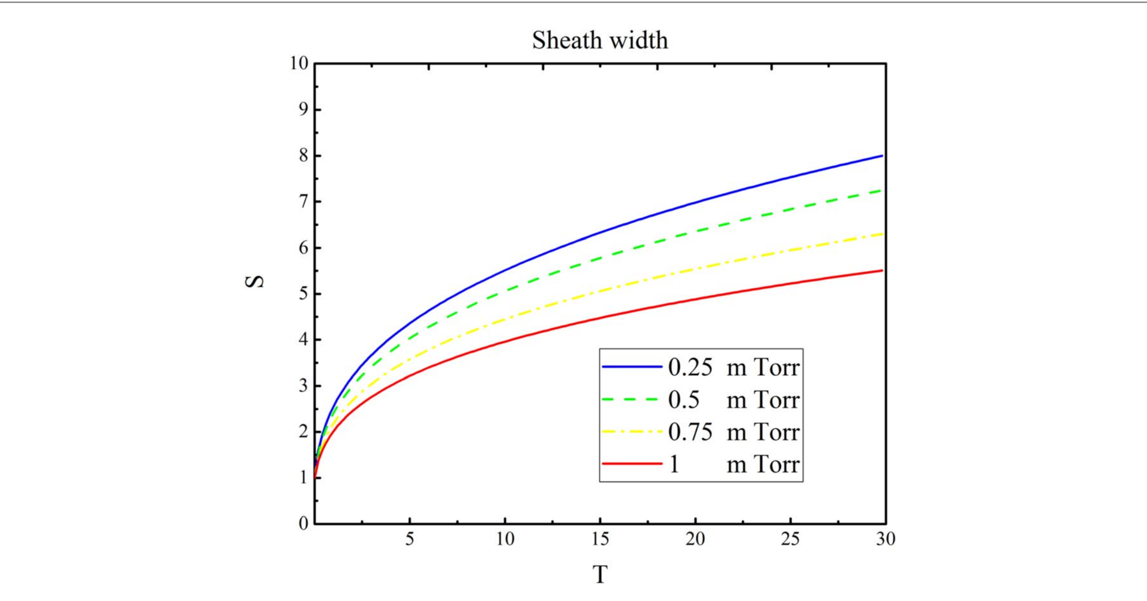


**Figure 8.** The normalized sheath width as a function of the normalized time for gas pressures of 0.25, 0.5, 0.75, and 1mTorr at the voltage of 6 kV.

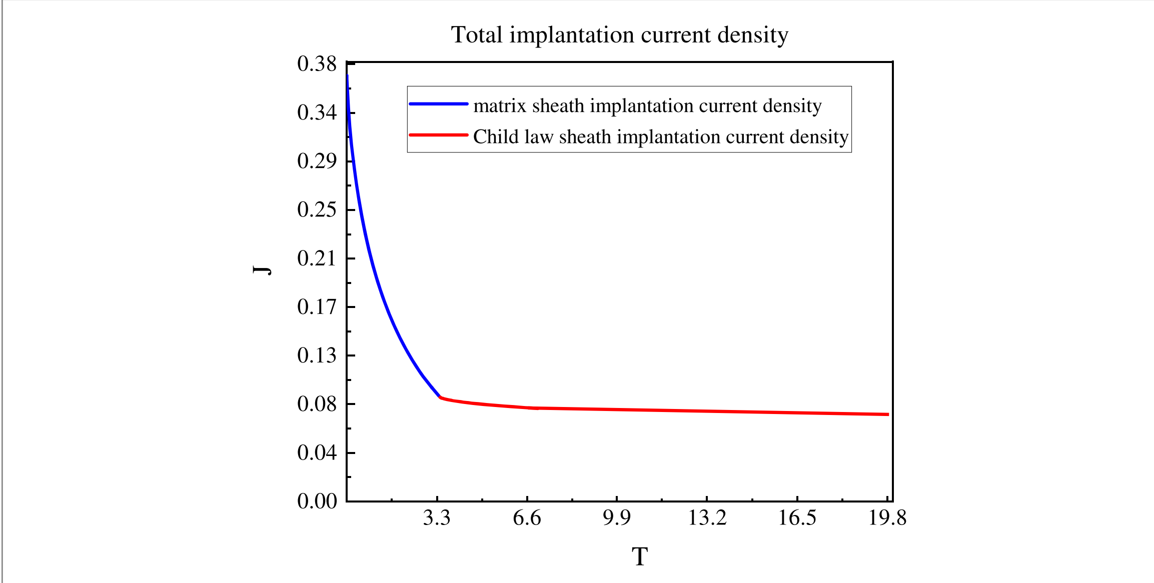


**Figure 9.** The normalized implanted current density, $J = j/en_0u_0$, versus the normalized time, $T = t\omega_pi$, at gas pressure of 0.4mTorr and voltage of 6 kV. Before $T < 3.4$ is matrix sheath ion implantation (equation (9)) and for $T > 3.4$ is Child law sheath ion implantation (equation (20)).

## 6. Summary and conclusion

In this paper, we have presented an analytical model to estimate the time-varying implantation current density and sheath width in the PSII process by considering the collisional effects. Using the presented model, we obtained dependence of the implantation current density and sheath width on applied voltage and gas pressure in the three different phases of collisional transient sheath evolution i.e., the initial matrix sheath, the expanding sheath, and the expanded sheath. The presented profiles of the implantation current density show that the collision parameter hasn't a restricting role on the ion motions in the initial phase of sheath evolution (the matrix sheath). However, in the expanding sheath, the collisional effects play an important role in the ion motion and the implanted current density. The applied voltage also has a significant effect on the implanted current density and the sheath thickness evolution. The total time-varying implantation current density during the collisional sheath evolution showed three different phases of the implantation process accurately. These results are of interest for many industrial applications to predict the collisional sheath dynamics in the process of surface treatment.

## Data availability statement

All data that support the findings of this study are included within the article (and any supplementary files).

## ORCID iDs

A R Niknam https://orcid.org/0000-0002-1460-7677
H Ghomi https://orcid.org/0000-0003-2203-5194

## References

[1] Conrad J R, Radtke J L, Doodd R A, Worzala F J and Tran N C 1987 *J. Appl. Phys.* **62** 4591
[2] Lieberman M A 1989 *J. Appl. Phys.* **66** 2926
[3] Liebermann M A and Lichtenberg A J 1994 *Principles of Plasma Discharges and Materials Processing* (New York: Wiley)
[4] Brutscher J, Günzel R and Moller W 1996 Sheath dynamics in plasma immersion ion implantation *Plasma Sources Sci. Technol.* **5** 54
[5] Pelletier J and Anders A 2005 *IEEE Trans. Plasma Sci.* **33** 6
[6] Lanterne A, Lerat J F, Michel T, Desrues T, Coig M, Milesi F, Mazen F, Veschetti Y, Roux L and Dubois S 2017 *Conference*
[7] Nikiforov S A, Kim G H and Rim G H 2003 *IEEE Trans. Plasma Sci.* **31** 94
[8] Veau A, Desrues T, Lanterne A, Bellanger P, Torregrosa F, Roux L, Kaminski-Cachopo A, Rafhay Q and Dubois S 2018 *Conference Paper in AIP* **1999** 110007
[9] Franklin R N and Snell J 2000 *J. Plasma Phys.* **64** 131
[10] Goeckner M J, Fetherston R P, Hitchon W N G, Horswill N C, Keiter E R, Shamim M M, Breun R A, Conard J R and Sheridan T E 1995 *Phys. Rev.* E **51** 3760
[11] Pelletier J and Anders A 1993 *Appl. Phys.* **74** 2986
[12] Wang D and Yu J Y 2005 *IEEE Trans. Plasma Sci.* **33** 6
[13] Hatami M M, Niknam A R and Shokri B 2009 *Vacuum* **83** S231
[14] Ghomi H, Sharifian M, Niknam A R and Shokri B 2006 *J. Appl. Phys.* **100** 113301
[15] Hatami M M, Niknam A R, Shokri B and Ghomi H 2008 *Phys. Plasmas* **15** 053508
[16] Benilov M S 2009 *Plasma Sources Sci, Technol.* **18** 1
[17] Sheridan T E and Petcu M-C 1995 *IEEE Trans. Plasma Sci.* **23** 865
[18] Riemann K-U 1997 *Phys. Plasmas.* **4** 4158
[19] Sheridan T E, Kwok T K and Chu P K 1998 *Appl. Phys. Lett.* **72** 1826
[20] Franklin R N and Snell J 2003 *J. Phys. D: Appl. Phys.* **36** 2821
[21] Mandl S and Manova D 2019 *Surf. Coat. Technol.* **365** 83–93
[22] Ghomi H and Khoramabadi M 2010 *J. Appl. Phys.* **108** 063302
[23] Hatami M M, Shokri B and Niknam A R 2009 *J. Phys. D: Appl. Phys.* **42** 025204
[24] Riemann K-U, Ehlemann U and Wiesemann K 1992 *J. Phys. D: Appl. Phys.* **25** 620
[25] Sheridan T E 1997 *Plasma Sources Sci. Technol.* **6** 91
[26] Ishikawaa M, Oura K, Miyamoto N and Wada M 2018 *AIP Conf. Proc.* **2052** 060005
[27] Hatami M M, Shokri B and Niknam A R 2008 *Phys. Plasmas* **15** 123501
[28] Godyak V A and Sternberg N 1990 *IEEE Trans. Plasma Sci.* **18** 159
[29] Chesnokov J M, Vasiliev A L, Lukichev V F and Rudenko K V 2017 *J. Phys.: Conf. Ser.* **471** 012049
[30] Gupta D 2011 *International Journal of Advancements in Technology* **2** 4
[31] Matsumoto N, Kinoshita H, Choi J and Kato T 2020 *Sci. Rep.* **10** 10037
[32] Hatami M M, Niknam A R and Shokri B 2009 *Vacuum* **83** 231234
[33] Benilov M S and Franklin R N 2002 *J. Plasma Phys.* **67** 163
[34] Valentini H B 2000 *Plasma Sources Sci. Technol.* **9** 574
[35] Moulick R and Goswami K S 2015 *Phys. Plasmas* **22** 033510
[36] Moulick R, Garg A and Kumar M 2021 *Contr. Plasma Phys.* **61** e202100047
[37] Wang D, Ma T and Deng X 1993 *J. Appl. Phys.* **74** 15
[38] Roth J R 2001 *Applications to Nonthermal Plasma Processing* (Philadelphia: IOP Publishing)